**Article type: Communication**

# Wide-angle tunable critical coupling in nanophotonic optical coatings with low-loss phase change material

*Kandammathe Valiyaveedu Sreekanth*, Patinharekandy Prabhathan, Apoorva Chaturvedi, Yulia Lekina , Song Han, Shen Zexiang , Edwin Hang Tong Teo, Jinghua Teng* and Ranjan Singh**

Dr. K. V. Sreekanth, Dr. J. Teng
Institute of Materials Research and Engineering, Agency for Science, Technology and Research (A*STAR), 2 Fusionopolis Way, Singapore, 138634 Singapore

Dr. P. Prabhathan, Dr. Y. Lekina, Prof. S. Zexiang, Prof. R. Singh
Division of Physics and Applied Physics, School of Physical and Mathematical Sciences, Nanyang Technological University, Singapore 637371, Singapore

Dr. P. Prabhathan, Dr. Y. Lekina, Prof. S. Zexiang, Prof. R. Singh
Centre for Disruptive Photonic Technologies, The Photonics Institute, Nanyang Technological University, Singapore 637371, Singapore

Dr. A. Chaturvedi, Prof. E. H. Tong Teo
School of Materials Science and Engineering, Nanyang Technological University, Singapore, 639798 Singapore

Dr. S. Han
ZJU-Hangzhou Global Science and Technology Innovation Center, Key Laboratory of Advanced Micro/Nano Electronic Devices & Smart Systems of Zhejiang, Zhejiang University, Hangzhou 311200, China

Prof. E. H. Tong Teo
School of Electrical and Electronics Engineering, Nanyang Technological University, 50, Nanyang Avenue, Singapore, 639798 Singapore

*E-mail: sreekanth@imre.a-star.edu.sg, jh-teng@imre.a-star.edu.sg, ranjans@ntu.edu.sg

**Keywords:** Optical coatings, Perfect absorbers, Phase change materials, Critical light coupling, Transition metal dichalcogenides, Modulators.

**Abstract**

Realizing perfect light absorption in stacked thin films of dielectrics and metals through critical light coupling has recently received intensive research attention. In addition, realizing ultrathin perfect absorber and tunable perfect absorber in the visible spectrum is essential for novel optoelectronics applications. However, the existing thin film stacks cannot show tunable perfect absorption in a wide-angle range. Here, we propose tunable perfect absorption from normal incidence to a wide-angle range ($0^o$ to $70^o$) by utilizing a two-layer stack consisting of a high refractive index low-loss dielectric on a high reflecting metal. We experimentally demonstrate this by depositing a thin layer of low-loss phase change material such as $Sb_2S_3$ on a thin layer of silver. This structure shows tunable perfect absorption with large spectral tunability in the visible wavelength. Furthermore, we demonstrate absorption enhancement in 2D materials by transferring monolayer $MoS_2$ on the stack, which shows 96% light absorption with enhanced photoluminescence. In addition, the thin film stack can work as a scalable phase modulator offering a maximum phase tunability of ~$140^o$ by changing the structural state of $Sb_2S_3$ from amorphous to crystalline.

## 1. Introduction

The recent research in thin film nanophotonics suggests the importance of using scalable thin film cavities based on metals and dielectrics as an alternative platform for metasurfaces.[1] Various thin film stacks have been proposed for different applications other than the conventional application of thin films as simple anti-reflection coatings, which include imaging [2], nonlinear optics [3], superlenses [4], and sensing [5]. In particular, engineering light absorption in thin film-based absorbers is vital for various applications such as structural coloring [6], heat-assisted magnetic recording [7], cancer therapy [8], photo-acoustic imaging [9], solar thermophotovoltaics [10], photodetectors [11], and optical switching.[12]

Thin-film absorbers work on the principle of critical coupling of light to the absorbers.[1] In fact, perfect light absorption is related with critical light coupling, which is due to the existence of nonzero losses in optical cavities. The critical light coupling condition satisfies when the absorption equals the sum of the reflection, transmission, and scattering. The transmission and scattering can be negligible by using relatively thick opaque materials with smooth top surfaces. Therefore, to realize critical light coupling in thin films it is essential to balance absorption and reflection. In thin film cavities, the reflection can be suppressed by thin-film interference, particularly through amplitude splitting destructive interference. As a result, the light is entirely trapped inside the cavity and is dissipated owing to the existence of losses. Two conditions such as phase and amplitude conditions must be concurrently satisfied to realize critical light coupling, that is, the interfering waves must be out of phase and of equal amplitude. As a result, the light inside the lossy medium will be trapped and the field energy will be dissipated completely. Different configurations including metal-dielectric-metal Fabry-Perot cavities [1], a lossy dielectric on a high reflectance metal [13], and a lossless dielectric on a low reflectance substrate [14] have been used to realize critical light coupling. However, most systems show perfect absorption only at an oblique incidence of light, and even though some show perfect absorption at normal incidence, they are highly incident angle-dependent. [11-19] It

is challenging to realize perfect absorption from normal incidence to a wide-angle range, e.g., 0º to 70º.

Moreover, it is crucial to realize tunable perfect absorption with thin-film stacks because they offer cost-effective and scalable optical devices for active nanophotonics applications. In this direction, different chalcogenide phase-change materials (PCMs) have been proposed to realize tunable perfect absorption in the visible to infrared wavelengths since they provide substantial refractive index change by switching the structural state of PCMs from amorphous to crystalline. [20-26] More importantly, the structural phase of PCMs can be reliably and repeatedly switched using optical or electrical pulses. [26-29] However, one of the limitations of existing PCM-based perfect absorbers is the significant reduction of resonant absorption by switching the PCM phase between amorphous and crystalline, [21-26] because the critical coupling conditions deviate with the phase change of PCM.

Here, we propose to solve the above stated two issues by employing a simple two-layer cavity. This work demonstrates tunable critical light coupling at normal incidence to a wide-angle range using a two-layer cavity system consisting of a high refractive index low-loss dielectric on a high reflecting metal. In particular, we experimentally demonstrate tunable perfect absorption in the visible wavelength in a wide-angle range from normal incidence to 70º by depositing a thin layer of phase change material such as stibnite ($Sb_2S_3$) on a thin layer of silver. We reveal two potential applications of the proposed cavity: (i) By selecting the lossless wavelength range of amorphous $Sb_2S_3$ and transferring monolayer $MoS_2$ flakes on the stack, we demonstrate 96% light absorption at a particular wavelength with enhanced photoluminescence, and (ii) By utilizing the polarization-dependent absorption feature of the tunable stack at higher angles of incidence, we demonstrate phase modulation of light with a maximum phase tunability of 140º by changing the structural state of $Sb_2S_3$ from amorphous to crystalline.

## 2. Results and Discussion

### 2.1 Design of tunable nanophotonic optical coatings

We investigate the proposed cavity comprising a high refractive index low-loss dielectric film on a lossy substrate. As shown in **Figure 1**a, the cavity consists of a thin dielectric layer with refractive index $n_d+ik_d$ and thickness $t_d$ on a high reflecting metal substrate (refractive index $n_s + ik_s$). Using transfer matrix method [30] (TMM), we calculate reflection at normal incidence (0º) to realize critical light coupling. In our calculations, the dielectric film's real and imaginary refractive index is varied from 0 to 5 and 0 to 1, respectively. The dielectric film thickness is set to 50 nm. The complex permittivity of high reflecting metal substrate is obtained from the Drude model, $\varepsilon_m = 1 - \left(\frac{\omega_p^2}{\omega(\omega+iv)}\right)$ with $\omega_p$= 15.3 eV and $v$=598.4 meV [31]. The critical light coupling occurs when the reflection turns into zero, that is, the light completely absorbed by the cavity. **Figure 1**b shows the calculated 2D map of reflection with varying refractive index ($n_d+ik_d$) of the dielectric layer at 520 nm wavelength. As can be seen, zero reflection is possible at normal incidence of light when the real and imaginary refractive index of the dielectric film is ~ 3.5 and ~0.2, respectively. However, slightly higher refractive index values are required when the operating wavelength increases (**Figure 1**c). It shows that a high refractive index low-loss dielectric film with an increase in refractive index values ($n$ & $k$) for increasing wavelength is required to achieve tunable critical coupling at normal incidence.

### 2..2 Experimental demonstration of wide-angle and tunable critical coupling

We propose to use a wide bandgap phase-change material such as $Sb_2S_3$ (SbS) for this purpose. In particular, the bandgap of $Sb_2S_3$ can be tuned in the visible wavelength range from 2.0 to 1.7 eV [26]. Note that as deposited $Sb_2S_3$ thin film is in an amorphous phase and it can be crystallized by annealing at 280 ºC. **Figure 2**a shows the measured real and imaginary refractive index ($n$ & $k$) of a thin layer of $Sb_2S_3$ in amorphous and crystalline phases, respectively. At <550 nm wavelength, $n$ of amorphous $Sb_2S_3$ varies from 3.4 to 3.7 with a $k$ value variation from 0.1 to 1.

However, both *n* and *k* values increase when the phase of the $Sb_2S_3$ is changed from amorphous to crystalline. It shows that $Sb_2S_3$ is a good candidate to be used as a high refractive index low-loss dielectric material.

Thin-film cavities were fabricated by the sequential deposition of Ag and $Sb_2S_3$ thin films on cleaned silicon and quartz substrates. Initially, a 100 nm thick Ag layer was deposited by thermal evaporation process, followed by the deposition of 90 nm thick $Sb_2S_3$ thin layer by sputtering technique (see Supporting Information). Reflection measurements at normal incidence and oblique incidence (25º-70º) were performed using a microspectrometer and variable angle spectroscopic ellipsometer, respectively (see Supporting Information). The measured reflection spectrum of an Ag/$Sb_2S_3$ stack at normal incidence is shown in **Figure 2**b. As can be seen, the Ag/$Sb_2S_3$ stack shows narrowband perfect absorption with a small reflection (<4%) at 550 nm (black curve). The observed small reflection is due to the scattering of the rough surface of the $Sb_2S_3$ thin layer. This scattering issue can be overcome by depositing a thin layer of ITO on the Ag/$Sb_2S_3$ stack. The ITO capping layer also helps to avoid the oxidation of the top $Sb_2S_3$ layer while doing crystallization by annealing the sample at 280 ºC. The reflection spectrum of an Ag/$Sb_2S_3$ (70 nm)/ITO (30 nm) stack for both amorphous and crystalline phases of $Sb_2S_3$ at normal incidence is shown in Figure 2b. Notably, zero reflection is obtained at 550 nm with an amorphous Ag/$Sb_2S_3$/ITO stack (red curve), evidencing the critical light coupling at normal incidence.

The tunable perfect absorption with a significant wavelength shift of 75±3 nm is obtained by changing the phase of $Sb_2S_3$ from amorphous to crystalline. The corresponding color change from pink to green is shown in the inset of **Figure 2**b. It should be noted that more than 95% light absorption is obtained even after crystallization of the sample. It shows that tunable critical coupling is possible with the proposed thin film coating, as the real and imaginary refractive indices of $Sb_2S_3$ thin layer increase with increase in wavelength. However, the existing PCM-based tunable cavities do not show this feature due to the deviation from the

critical coupling condition [21-26]. We then calculated the reflection spectrum of the three stacks at normal incidence using the transfer matrix method. The calculated results shown in **Figure 2**c correlate well with the experimental results. In our calculations, experimentally determined optical constants of $Sb_2S_3$ (Fig. 2a), Ag and ITO (see Supporting Information Fig. S1) were used.

We studied the influence of incident angle and polarization on the perfect absorption feature of the stacks. In **Figure** 3, we report the calculated (0º to 70º) and measured (25º to 70º) angular reflection spectra of the Ag/$Sb_2S_3$ stack for both *p*- and *s*-polarizations. A wide-angle perfect absorption is obtained for *p*-polarization from 0º to 70º, however, *s*-polarization does not show perfect absorption above 50º. The observed wide-angle perfect absorption is due to the high refractive index of the $Sb_2S_3$ layer. The effect of incident angle and polarization on the tunable perfect absorption feature of Ag/$Sb_2S_3$/ITO stack is shown in Supporting Information Fig. S2. Moreover, the observed polarization-dependent wide-angle tunable perfect absorption is due to the Brewster effect and the amplitude splitting destructive interference needed to realize perfect absorption. In particular, the Fresnel reflection coefficient of *p*-polarized light at the air/dielectric ($Sb_2S_3$) interface decreases up to Brewster angle and then increases as it approaches 90º, however, the Fresnel reflection coefficient of *s*-polarized light keeps increases with increasing incident angle (0º to 90º) (see Supporting Information Fig. S3). Also note that the perfect absorption wavelength blue shifts with increasing incident angle for *p*-polarization. This is because the optical path difference decreases with increasing incident angle, as a result wavelength blue shifts to satisfy the destructive interference condition. Since the stacks show incident angle independent perfect absorption, angle independent color tunability is realized (Figure 2b inset), which is important for structural coloring applications. Moreover, the observed polarization-dependent tunable perfect absorption feature at higher angles of incidence (above 50º) can be used to realize scalable visible wavelength phase modulators.

The critical light coupling is realized for the proposed stacks by satisfying both amplitude and phase conditions. The amplitude condition is satisfied by maximizing the optical absorption inside the $Sb_2S_3$ layer (see Supporting Information Fig. S4). The reflection amplitude from both the dielectric and the metal layer can be equal as the low-loss dielectric dampens the magnitude of the partially reflected light from the high reflecting metal [1]. The required phase condition for optimum dielectric thickness ($t_{opt}$) is, $t_{opt} = n_d t_d = \lambda/2$, where $n_d$ and $t_d$ are the refractive index and thickness of dielectric layer and $\lambda$ is the wavelength of light. This phase condition is like in metal–dielectric–metal (MDM) cavities [1]. However, the entire light is trapped inside the $Sb_2S_3$ layer in the proposed cavity whereas the absorption in an MDM cavity is distributed between the two metal layers [1]. The observed absorption characteristic of the proposed stack could find many applications that demand concentrating light absorption entirely in a dielectric layer. Moreover, the proposed tunable cavity has several advantages over PCM based MDM cavities [21-26], e.g., it is oxidation resistant due to the dielectric capping layer and provides tunable perfect absorption from normal incidence to a wide-angle range.

**2.3 Experimental demonstration of a 2D material based perfect absorber**

Direct bandgap monolayer two-dimensional (2D) semiconductor materials have recently received great attention in novel optoelectronic device application. [32] However, it is essential to improve the absorption of monolayers in optical devices utilizing 2D semiconductor materials. [33] Various light trapping schemes including thin film cavities were proposed for this purpose. [34-37] Among these, a lossless dielectric on high reflectance metal is the attractive thin film coating for increasing the absorption cross-section of an ultrathin absorbing layer. [36] In an ultrathin absorbing film-coated cavity, the ultrathin absorbing film can dissipate the trapped light with high power dissipation density values. [1] This method has been widely used to maximize the absorption and hence the photoluminescence from various 2D monolayer transition metal dichalcogenides (TMDs). [38-41] Moreover, near-unity absorption of monolayer TMDs at low temperatures (90% absorption below 200 K) and by transferring multiple layers

of TMDs on various substrates were realized. [42-45] However, a monolayer TMD based perfect absorber operating at room temperature has not yet been realized. It is important to note that absorption enhancement of ultrathin absorbing film can be engineered by tuning the refractive index of the lossless dielectric layer. Here, we propose to realize a 2D material based perfect absorber operating at room temperature by transferring monolayer $MoS_2$ flakes on $Ag/Sb_2S_3$ stack.

Among 2D materials, monolayer $MoS_2$ provides maximum optical absorption in the visible wavelength range, 2-5%. Even higher optical absorption of 5-10% is possible at certain wavelengths in the visible spectrum due to excitonic excitations. [41] One way is to increase the absorption at the excitonic absorption bands (A and B) of $MoS_2$, above 600 nm wavelength, is to couple with an optical cavity. [39-40] Since $Sb_2S_3$ thin film in the amorphous phase shows lossless behavior above 600 nm wavelength, $Ag/Sb_2S_3$ stack provides a cavity of lossless dielectric on a high reflectance metal. **Figure 4**a illustrates the schematic of the proposed ultrathin perfect absorber consisting of monolayer $MoS_2$ on an $Ag/Sb_2S_3$ (amorphous) stack. We synthesized $MoS_2$ monolayers through chemical vapor deposition and later exfoliated (transferred) on to the stack of $Ag/Sb_2S_3$ by using the poly (methyl methacrylate) (PMMA) nanotransfer method as described in Ref [46, 47]. The optical microscopic image of many monolayer $MoS_2$ on an $Ag/Sb_2S_3$ stack is shown in **Figure 4**b. A microspectrometer was used to measure the reflection spectrum of $Ag/Sb_2S_3/MoS_2$. The measured absorption spectrum of $Ag/Sb_2S_3$ and $Ag/Sb_2S_3/MoS_2$ at normal incidence is shown in **Figure 4**c. The absorption peak of $Ag/Sb_2S_3$ stack is located at a wavelength of 550 nm, however, the absorption peak of $Ag/Sb_2S_3/MoS_2$ is red shifted to 620 nm. In particular, the absorption peak of $Ag/Sb_2S_3/MoS_2$ is obtained at the B excitonic band of $MoS_2$. Since the cavity absorption of $Ag/Sb_2S_3$ is < 20% at 620 nm, the achieved 96% light absorption of $Ag/Sb_2S_3/MoS_2$ is solely due to monolayer $MoS_2$ because $MoS_2$ exhibits a vital excitonic feature even at room temperature.

The calculated absorption spectrum of both stacks is shown in **Figure 4**d, which correlates well with the experimental results. The simulated electric field distribution of the $Ag/Sb_2S_3/MoS_2$ stack at 620 nm shows that the electric field is tightly confined at the $Sb_2S_3/MoS_2$ interface (Supporting Information Fig. S5). Moreover, we calculated the absorption spectrum of $MoS_2$ on Ag, $Ag/TiO_2$ and $Ag/SiO_2$ at normal incidence (Supporting Information Fig. S6). These results further confirm that the experimentally obtained absorption peak of $Ag/Sb_2S_3/MoS_2$ at 620 nm is due to B excitonic excitation. In our simulations, the thickness of monolayer $MoS_2$ was assumed to be 1 nm and the optical constants of $MoS_2$ were obtained from Ref [48, 49].

We further confirmed enhanced absorption of monolayer $MoS_2$ by performing photoluminescence (PL) measurement (see Supporting Information for the experimental details). The PL spectrum (632.8 nm excitation) of $Si/Ag/Sb_2S_3/MoS_2$ and reference ($Si/Sb_2S_3/MoS_2$) samples are presented in **Figure 4**e. The experimental spectra were fitted using Lorentzian line shape. The $Ag/Sb_2S_3/MoS_2$ sample exhibits a 15-fold increase in PL intensity with respect to the reference sample. The considered reference sample ($Si/Sb_2S_3/MoS_2$) is a $MoS_2$ coupled lossless dielectric on a low reflectance substrate [14], which also acts as a cavity system. By considering this fact and the excitation wavelength, obtained PL enhancement is substantial compared to previously reported cavities. [37-40] The observed enhanced PL intensity is due to the enhanced absorption of $MoS_2$ at 632.8 nm excitation laser wavelength. The laser power-dependent PL enhancement of $Ag/Sb_2S_3/MoS_2$ cavity was also investigated (see Supporting Information Fig. S7). In short, the demonstrated perfect absorption with enhanced photoluminescence from a monolayer $MoS_2$ coupled cavity could find potential applications in developing thin photovoltaics [30], photodetectors, light-emitting devices, and lasers.

**2.4 Experimental demonstration of a scalable phase modulator**

The phase modulation of light could find many applications including light detection and ranging, optical switching fabrics, artificial neural networks, free-space optical communication,

and phased-array imaging. [50] The tunable metasurfaces based on different technologies including field-effect tunability and PCMs have been proposed to realize phase modulators for different spectral bands. [51] However, thin-film cavities can be used to develop scalable reflective phase modulators, like graphene, and superconductor-based tunable thin-film cavity devices have been proposed for reflective phase modulation at terahertz frequencies. [52, 53] Recently, continuously tunable reflection amplitude in the near infrared wavelength was experimentally demonstrated using a PCM-based thin film stack. [54] Here, we use the polarization dependent feature of the proposed stack at higher angles of incidence (>50º) to realize PCM based tunable reflective phase modulators at visible wavelengths, which could find exciting applications such as optical sensing, nonlinear optics and optogenetics. [55]

The measured angular (25º to 80º) differential phase spectra (phase difference between *p*- and *s*-polarization) of Ag/$Sb_2S_3$/ITO stack in amorphous and crystalline phases are shown in **Figure 5**a and b, respectively. A variable angle spectroscopic ellipsometer was used to measure the phase spectra. In the visible wavelength (400-800 nm), the phase variation from 0º to 180º is obtained at higher angles of incidence (>60º) for amorphous Ag/$Sb_2S_3$/ITO stack, however, crystalline Ag/$Sb_2S_3$/ITO stack shows almost constant phase variation. In particular, a sudden phase jump occurred at the Brewster angle (62º) of the amorphous Ag/$Sb_2S_3$/ITO stack. This phase-jump property across the Brewster angle provides deep phase modulation when the phase of the $Sb_2S_3$ in the stack is changed from amorphous to crystalline. **Figure 5**c shows the measured *p*- and *s*-polarized reflection spectrum of Ag/$Sb_2S_3$/ITO stack in both amorphous and crystalline phases at 62º incident angle. In the case of an amorphous stack, almost zero reflection and above 10% reflection are obtained for *p*- and *s*-polarization at a wavelength of 530 nm, respectively. As a result, an abrupt change in phase is obtained at the Brewster angle, as shown in **Figure 5**d. However, a constant phase variation is obtained for crystalline stack at the Brewster angle. This is due to the increase of *p*-polarized reflection at 530 nm wavelength. It shows that a maximum reflective phase modulation of 140º is obtained at the Brewster angle

(62º) by switching the $Sb_2S_3$ phase from amorphous to crystalline. We confirmed the obtained experimental results using a TMM based numerical simulation model (see Supporting Information Fig. S8). While the stack shows the maximum phase modulation at the Brewster angle, above 100º phase modulation is still possible by selecting an incident angle around the Brewster angle. The electrical continuous tuning of reflected phase with reversible tunability is possible by integrating the thin film stack with a microheater device [56-58] and it could be a promising platform for flat optics applications. [59]

## 3. Conclusion

We experimentally demonstrated a 2D material based perfect absorber and a scalable reflective phase modulator by critical coupling of light in tunable nanophotonic cavities. We showed narrowband tunable perfect absorption in the visible wavelength range from normal incidence to a wide-angle range of 70º by stacking a high refractive index and low-loss phase change material such as $Sb_2S_3$ on top of a Ag film. A broad spectral tunability of 75±3 nm with angle-independent color generation is realized. A 2D material based perfect absorber is realized by transferring monolayer $MoS_2$ flakes onto the stack, which showed 96% light absorption with enhanced photoluminescence. By exploiting the phase jump property across the Brewster angle and the structural phase switching of $Sb_2S_3$ layer from amorphous to crystalline, a reflective phase modulator with a phase tunability of 140±5º is realized at a particular wavelength.

## 4. Experimental Section

*Sample fabrication:* Thin film samples were fabricated by the sequential deposition of Ag, $Sb_2S_3$, and ITO thin films on silicon and quartz substrates. The substrates were pre-cleaned using acetone, ethanol, and deionized water prior to deposition. The thin layer of Ag was deposited using thermal evaporation technique. RF magnetron sputtering was used to deposit thin layers of $Sb_2S_3$ and ITO. The distance between the substrate and target was kept 15 cm to achieve uniform deposition of thin films. The deposition was carried out at room temperature

at a fixed RF power of 70 Watt under the high purity argon (99.999%) atmosphere at deposition pressure of 10 mTorr.

*$MoS_2$ fabrication and transfer:* $MoS_2$ monolayers were synthesized using chemical vapor deposition and transferred onto the stack of $Ag/Sb_2S_3$ by using the PMMA nanotransfer method.

*Ellipsometer characterization:* Variable-angle spectroscopic ellipsometer (J. A. Woollam Co., Inc, V-VASE) was used to determine the thicknesses and the optical constants of grown thin films of $Sb_2S_3$, Ag and ITO. Angular phase spectrum ($\Delta$) was acquired using the VASE ellipsometer. The ellipsometer phase spectrum is the phase difference between *p*-and *s*-polarizations.

*Reflection measurements:* Angular reflectance spectrum for both *p*- and *s*-polarizations were measured using the variable-angle spectroscopic ellipsometer (J. A. Woollam Co., Inc, V-VASE). The transmittance is zero for all wavelengths and angles. Since we are dealing with thin films, perfect light absorption corresponds to near zero reflectance. The normal incidence reflectance measurements were performed using a microspectrophotometer (Jasco, MSV-5200) with a sampling domain size of 15 μm ×15 μm and a numerical aperture of 0.7.

*PL measurements:* A WITec Alpha 300RAS confocal Raman microscope was used to record photoluminescence (PL) spectra. The He−Ne laser with the 632.8 nm (red) wavelength was chosen as an excitation source to match the perfect absorption region. A 100x Olympus objective with NA0.95 and the laser spot size of ~ 1 μm was used. Excitation power was kept in the range from 0.5 to 65 μW to obtain a sufficient signal but to avoid degradation of the samples. The signal was collected in backscattered geometry with an Acton spectrometer with a diffraction grating of 150 grooves/mm and a thermo-electrically cooled Andor CCD detector. The PL signal passed through two 633 nm BragGrate Notch Filters (BNF) for effective laser line rejection.

*Numerical simulations:* Reflectance spectra and field distribution plots were simulated using transfer-matrix-method (TMM) code written in MATLAB.

***Statistical analysis***: All experiments were performed in triplicate and the data such as wavelength shift and phase shift are expressed as the mean ± standard deviation. The Origin software was used for the data analysis.

**Supporting Information**

Supporting Information is available from the Wiley Online Library or from the author.

**Acknowledgements:**

The authors (P. P. and R. S.) acknowledge the funding support from Advanced Manufacturing and Engineering (AME) Programmatic grant (A18A5b0056) by Agency for Science, Technology, and Research (A*STAR). K. V. S. and J.T acknowledge A*STAR for funding support in Grant Nos. H19H6a0025, A20E5c0084, A2083c0058 and CRF SC25/21-110318.

**Conflict of Interest**

The authors declare no conflict of interest.

**Data Availability Statement**

The data that support the findings of this study are available from the corresponding author upon reasonable request.

**References**

[1] K. V. Sreekanth, M. ElKabbash, V. Caligiuri, R. Singh, A. De Luca, G. Strangi, *New Directions in Thin Film Nanophotonics*, Springer, New York 2019.

[2] O. Reshef, M. P. DelMastro, K. K. M. Bearne, A. H. Alhulaymi, L. Giner, R. W. Boyd, J. S. Lundeen, *Nat. Commun.* **2021**, 12, 3512

[3] Y. Zhao, Y. Yang, H.-B. Sun, *PhotoniX* **2021**, 2, 3.

[4] V. Caligiuri, R. Dhama, K. V. Sreekanth, G. Strangi, A. De Luca, *Sci Rep* **2016**, 6, 20002

[5] K. V. Sreekanth, Y. Alapan, M. ElKabbash, E. Ilker, M. Hinczewski, U. A. Gurkan, A. De Luca, G. Strangi, *Nat. Mater.* **2016**, 15, 621

[6] M. ElKabbash, S. Iram, T. Letsou, M. Hinczewski, G. Strangi, *Adv. Opt. Mater*. **2018**, 6, 18

[7] G. Ju, Y. Peng, E. K. C. Chang, Y.Ding, A. Q. Wu, X. Zhu, Y. Kubota, T. J. Klemmer, H. Amini, L. Gao, Z. Fan, T. Rausch, P. Subedi, M. Ma, S. Kalarickal, C. J. Rea, D. V. Dimitrov, P.-W. Huang, K. Wang, X. Chen, C. Peng, W. Chen, J. W. Dykes, M. A. Seigler, E. C. Gage, R. Chantrell, J.-U. Thiele, *IEEE Trans Magn* **2015**, 51, 1

[8] X. Huang, M. A. El-Sayed, *Alexandria J Med*. **2011**,47,1

[9] C. Tian, W. Qian, X. Shao, Z. Xie, X. Cheng, S. Liu, Q. Cheng, B. Liu, X. Wang, *Adv. Sci*. **2016**, 3, https://doi.org/10.1002/advs.201670065

[10] D. M. Bierman, A. Lenert, W. R. Chan, B. Bhatia, I. Celanovi´c, M. Solja˘ci´c, E. N. Wang, *Nat. Energy* **2016**, 1,16068

[11] M. A. Kats, F. Capasso, *Laser Photonics Rev.* **2016**, 10, 735.

[12] Y. Yang, K. Kelley, E. Sachet, S. Campione, T. S. Luk, J. -P. Maria, M. B. Sinclair, I. Brener, *Nat. Photon*. **2017**, 11, 390

[13] M. A. Kats, R. Blanchard, P. Genevet, F. Capasso, *Nat. Mater.* **2013**, 12, 20

[14] a) M. ElKabbash E. Ilker, T. Letsou, N. Hoffman, A. Yaney, M. Hinczewski, G. Strangi, *Opt. Lett*. **2017**, 42, 3598; b) M. El Kabbash, A. R. Rashed, K. V. Sreekanth, A. De Luca, M. Infusino, G. Strangi, *Journal of Nanomaterials* **2016,** 4819040

[15] K. V. Sreekanth, S. Sreejith, S. Han, A. Mishra, X. Chen, H. Sun, C. T. Lim, R. Singh, *Nat. Commun*. **2018**, 9, 369

[16] Z. Li, S. Butun, K. Aydin, *ACS Photonics* **2015**, 2, 183

**[**17**]** H. Kocer, S. Butun, Z. Li, K. Aydin, *Sci. Rep*. **2015**, 5, 8157

[18] a) K. V. Sreekanth, M. ElKabbash, R. Medwal, J. Zhang, T. Letsou, G. Strangi, M. Hinczewski, R. S. Rawat, C. Guo, R. Singh, *ACS Photonics* **2019**, 6, 1610; b) K. V. Sreekanth, S. Sreejith, Y. Alapan, M. Sitti, C. T. Lim, R. Singh, *Adv. Opt. Mater*. **2019**, 7, 1801313.

[19] H. Song, L. Guo, Z. Liu, K. Liu, X. Zeng, D. Ji, N. Zhang, H. Hu, S. Jiang, Q. Gan, *Adv. Mater*. **2014**, 26, 2737

[21] M. Wuttig, H. Bhaskaran, T. Taubner, *Nat. Photonics* **2017**, 11, 465

[20] a) K. V. Sreekanth, S. Han, R. Singh, *Adv. Mater*. **2018**, 30, 1706696; b) K. V. Sreekanth, P. Mahalakshmi, S. Han, M. S. Mani Rajan, P. K. Choudhury, R. Singh, *Adv. Opt. Mater*. **2019**, 7, 1900680

[23] A. Heßler,I. Bente, M. Wuttig, T. Taubner, *Adv. Opt. Mater*. **2021**, 9, 2101118

[24] V. K. Mkhitaryan, D. S. Ghosh, M. Rudé, J. Canet-Ferrer, R. A. Maniyara, K. K. Gopalan, V. Pruneri, *Adv. Opt. Mater*. **2017**, 5, 1600452

[25] S. K. Chamoli, G. Verma, S.C. Singh, C. Guo, *Nanotechnology* **2021**, 32, 095207

[26] a) W. Dong, H. Liu, J. K. Behera, L. Lu, R. J. H. Ng, K. V. Sreekanth, X. Zhou, J. K. W. Yang, R. E. Simpson, *Adv Funct Mater* **2019**, 29, 1806181; b) K. V. Sreekanth, Q. Ouyang, S. Sreejith, S. Zeng, W. Lishu, E. Ilker, W. Dong, M. ElKabbash, Y. Ting, C. T. Lim,

M. Hinczewski, G. Strangi, K. T. Yong, R. E. Simpson, R. Singh, *Adv. Opt. Mater*. **2019**, 7, 1900081

[27] Q. Wang, R. T. F. Edward, G. Behrad, W. Chih-Ming, Y. Guanghui, T. Jinghua, Z. I. Nikolay, *Nat. Photon.* **2016**, 10, 60

[28] Y. Zhang, C. Fowler, J. Liang, B. Azhar, M. Y. Shalaginov, et al., *Nat. Nanotechnol.* **2021**, 16, 661

[29] Y. Wang, P. Landreman, D. Schoen, K. Okabe, A. Marshall, U. Celano, H.-S. P. Wong, J, Park, M. L. Brongersma, *Nat. Nanotechnol.* **2021**, 16, 667

[30] W. N. Hansen, *J. Opt. Soc. Am.* **1968**, 58, 380.

[31] M. G. Blaber, M. D. Arnold, M. J. Ford, *J. Phys. Chem. C* **2009**, 113, 3041

[32] Y. Li, Z. Li, C. Chi, H. Shan, L.Zheng, Z. Fang, *Adv. Sci*. 2017, 4, 1600430

[33] D. Jariwala, A. R. Davoyan, J. Wong, H. A. Atwater, *ACS Photonics* **2017**, 4, 2962

[34] Q. Hao, J. Pang, Y. Zhang, J. Wang, L. Ma, O. G. Schmidt, *Adv. Opt. Mater*. **2018**, 6, 1700984

[35] H. Song, L. Guo, Z. Liu, K. Liu, X. Zeng, D. Ji, N. Zhang, H. Hu, S. Jiang, Q. Gan, *Adv Mater*. **2014**, 26,2737

[36] J. R. Tischler, M. S. Bradley, V. Bulovi´c, *Opt. Lett.* **2016,** 31, 2045

[37] L. Zhu, F. Liu, H. Lin, J. Hu, Z. Yu, X. Wang, S. Fan, *Light: Science & Applications* **2016**, 5, e16052; doi:10.1038/lsa.2016.5

[38] D. H. Lien, J. S. Kang, M. Amani, K. Chen, M. Tosun, H. P. Wang, T. Roy, M. S. Eggleston, M. C. Wu, M. Dubey, S. C. Lee, J. H. He, A. Javey, *Nano Lett*. **2015, 15,** 1356−1361

[39] J. T. Liu, T. B. Wang, X. J. Li, N. H. Liu, *J. Appl. Phys*. **2014**, 115, 193511

[40] H. Y. Jeong, U. J. Kim, H. Kim, G. H. Han, H. Lee, M. S. Kim,Y. Jin, T. H. Ly, S. Y. Lee, Y.-G. Roh, W.-J. Joo, S. W. Hwang, Y. Park,Y. H. Lee, *ACS Nano* **2016,** 10, 8192

[41] V. G. Kravets, F. Wu, G. H. Auton, T. Yu , S. Imaizumi, A. N. Grigorenko, *npj 2D Mater Appl* **2019, 3,** 36. https://doi.org/10.1038/s41699-019-0119-1

[42] J. Horng, E. W. Martin,Y.-H. Chou, E. Courtade, T.-c. Chang, C.-Y. Hsu, M.-H. Wentzel, H. G. Ruth, T.-c. Lu, S. T. Cundiff, F Wang, H.Deng, *Phys. Rev. Applied* **2020**, 14, 024009

[43] D. Jariwala, A.R. Davoyan, G. Tagliabue, M. C. Sherrott, J. Wong, H. A. Atwater, *Nano Lett*. **2016**, 16, 5482-5487

[44] I. Epstein, B. Terres, A. J. Chaves, V.-V. Pusapati, D. A. Rhodes, B. Frank, V. Zimmermann, Y. Qin, K. Watanabe, T. Taniguchi, H. Giessen, S. Tongay, J. C. Hone, N. M. R. Peres, F. H. L. Koppens, *Nano Lett*. **2020**, 20, 3545-3552.

[45] K. F. Mak, C. Lee, J. Hone, J. Shan, T. E. Heinz, *Phys. Rev. Lett*. **2010**, 105, 136805.

[46] B. Li, S. Zu, J. Zhou, Q. Jiang, B. Du, H. Shan, Y. Luo, Z. Liu, X. Zhu, Z. Fang, *ACS Nano* **2017**, 11, 9720-9727

[47] M. Amani, R. A. Burke, X. Ji, P. Zhao, D. H. Lien, P. Taheri, G. H. Ahn, D. Kirya, .J. W. Ager III, E. Yablonovitch, J. Kong, *ACS nano* **2016**., 10, 6535-6541

[48] A. R. Bea, H. P. Hughes, *J. Phys. C: Solid State Phys.* **1979**, 12, 881

[49] Y. Li, A. Chernikov, X. Zhang, A. Rigosi, H. M. Hill, A. M. van der Zande, D. A. Chenet, E.-M. Shih, J. Hone, T. F. Heinz, *Phys. Rev. B* **2014**, 90, 205422

[50] C. Sturm, D. Tanese, H. S. Nguyen, H. Flayac, E. Galopin, A. Lemaitre, I. Sagnes, D. Solnyshkov, A. Amo, G. Malpuech, J. Bloch, *Nat. Communications* **2014**, 5, 3278

[51] Q. Song, *Light: Science & Applications* **2021**, 10, 184.

[52] K. V. Sreekanth, P. Mahalakshmi, S. Han, D. Vigneswaran, M. S. Mani Rajan, R. Jha, R. Singh, : *J. Appl. Phys.* **2020**, 128, 173106

[53] Z. Chen, X. Chen, L. Tao, K. Chen, M. Long, X. Liu, K. Yan, R. I. Stantchev, E. Pickwell-MacPherson, J.-B. Xu, *Nat. Commun*. **2018**, 9, 4909.

[54] S. Cueff, A. Taute, A. Bourgade, J. Lumeau, S. Monfray, Q. Song, P. Genevet, B. Devif, X. Letartre, L. Berguiga, *Adv. Opt. Mater*. **2021**, 9, 2001291

[55] G.Liang, H. Huang, A. Mohanty, M. C. Shin, X. Ji, M. J. Carter, S. Shrestha, M. Lipson, N. Yu, *Nat. Photon.* **2021**, 15, 908–913

[56] a) K. V. Sreekanth, R Medwal, Y Kumar Srivastava, M Manjappa, R. S. Rawat R. Singh, *Nano Letters* **2021**, 21, 10070–10075; b) K. V. Sreekanth, R Medwal, C. M. Das, M. Gupta, M. Mayank, K. T. Yong, R. S. Rawat R. Singh, *Nano Letters* **2021**, 21, 4044–4050

[57] K. V. Sreekanth, C. M. Das, R. Medwal, M. Mayank, Q. Ouyang, R. S. Rawat, K. T. Yong, R. Singh, *Adv. Mater*. **2021**, 33, 2006926

[58] Y. Wang, P. Landreman, D. Schoen, K. Okabe, A. Marshall, U. Celano, H.-S. P. Wong, J. Park, M. L. Brongersma, *Nat. Nanotechnol.* **2021**, 16, 667–672

[59] J. Ni, C. Huang, L.-M. Zhou, M. Gu, Q. Song, Y. Kivshar, C.-W. Qiu, Science 2021, 374, eabj0039

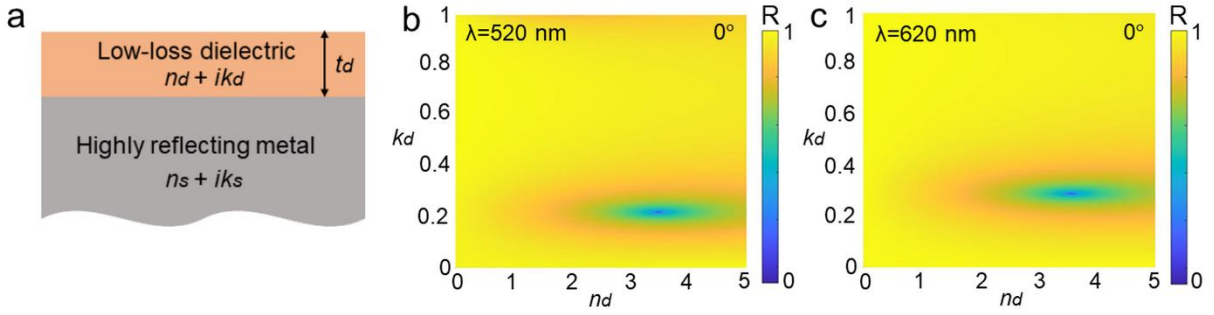


**Figure 1** Critical coupling of light in a two-layer cavity (a) Schematic of the proposed cavity consisting of a low-loss dielectric film on a highly reflecting metal substrate. Calculated 2D map of reflection spectrum at normal incidence as a function of the real and imaginary refractive index of dielectric film for (b) 520 nm and (c) 620 nm

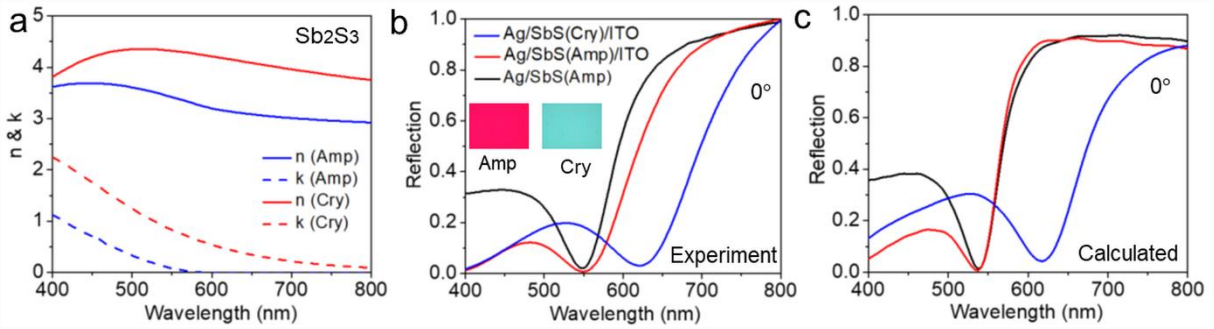


**Figure 2** Experimental demonstration of tunable critical light coupling at normal incidence (a) Measured optical constants of $Sb_2S_3$ thin film in amorphous and crystalline phases. The reflection spectrum of amorphous Ag/$Sb_2S_3$, amorphous Ag/$Sb_2S_3$/ITO and crystalline Ag/$Sb_2S_3$/ITO stacks at normal incidence (b) measured and (c) calculated. Optical microscope image of the amorphous Ag/$Sb_2S_3$/ITO and crystalline Ag/ $Sb_2S_3$/ITO stack is shown in the inset of b. Amp: amorphous and Cry: crystalline

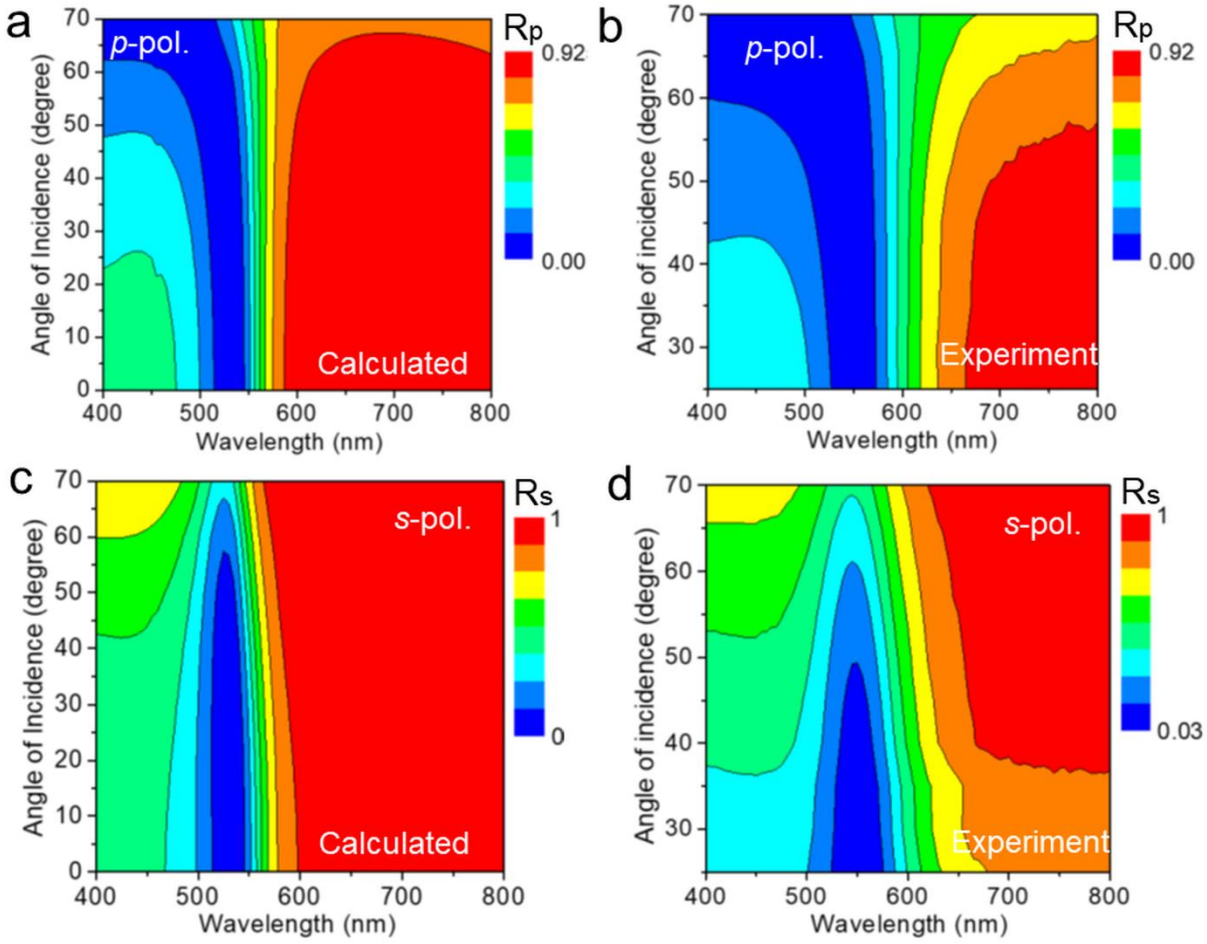


**Figure 3** Experimental demonstration of critical light coupling at wide angle range. Angular reflection spectrum of $Ag/Sb_2S_3$ stack for *p*-polarization (a) Calculated (0º to 70º) and (b) Measured (25º to 70º). Angular reflection spectrum of $Ag/Sb_2S_3$ stack for *s*-polarization (c) Calculated (0º to 70º) and (d) Measured (25º to 70º)

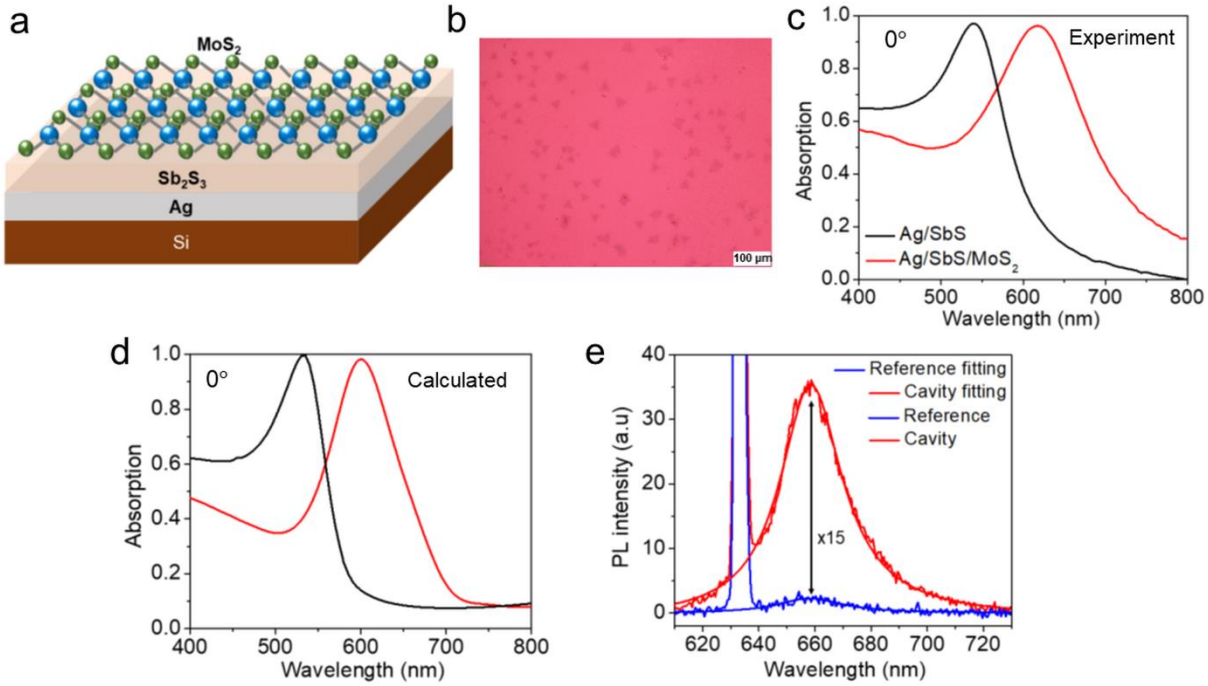


**Figure 4** Experimental demonstration of absorption enhancement in monolayer $MoS_2$ (a) Schematic of monolayer $MoS_2$ transferred $Ag/Sb_2S_3$ stack. (b) Optical microscope image of monolayer $MoS_2$ flakes on the stack. Absorption spectrum of $Ag/Sb_2S_3$ and $Ag/Sb_2S_3/MoS_2$ stack at normal incidence (c) Measured and (d) Calculated. (e) Photoluminescence spectra of cavity ($Si/Ag/Sb_2S_3/MoS_2$) and reference ($Si/Sb_2S_3/MoS_2$) samples collected under 633 nm excitation with a laser power of 5 μW

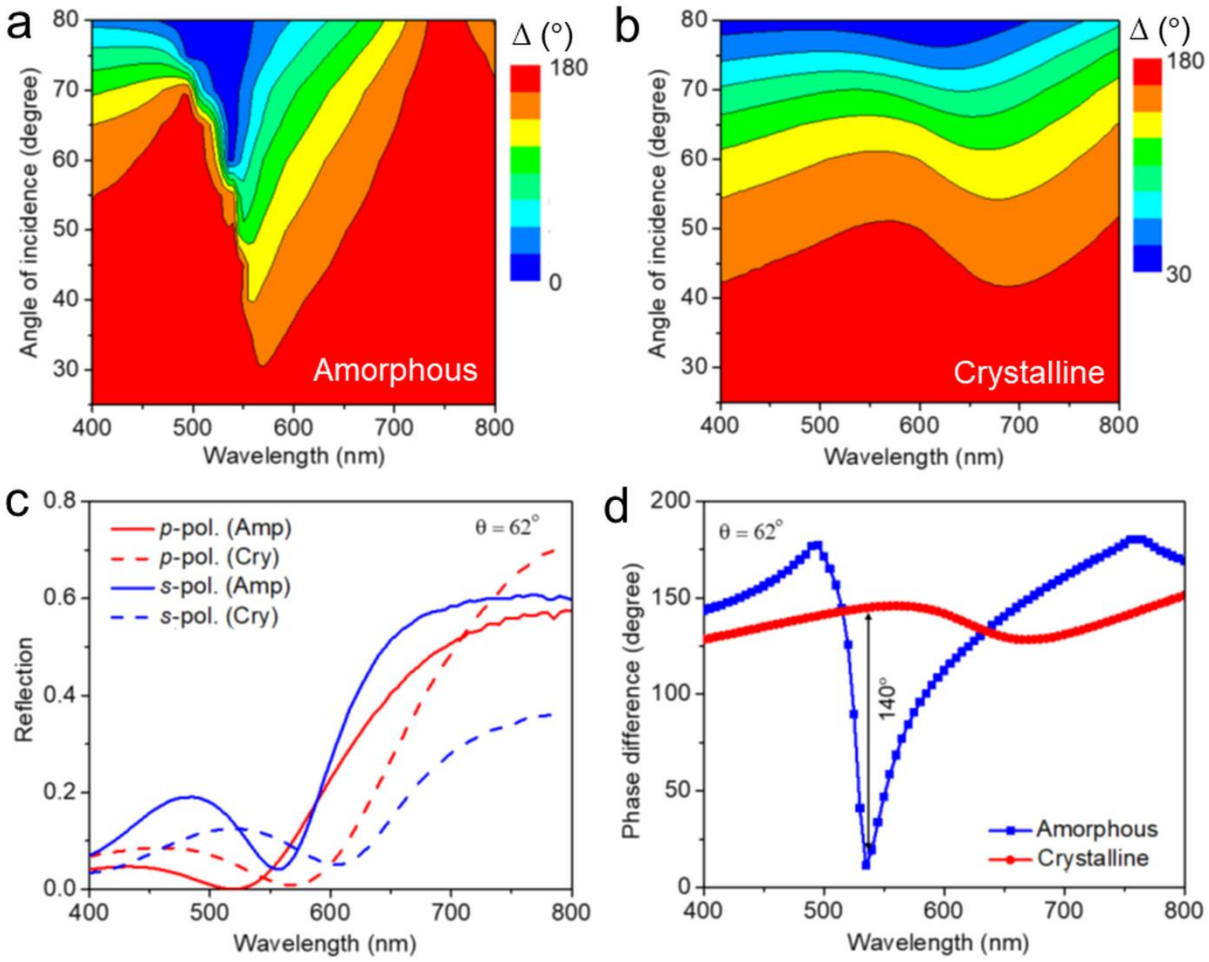


**Figure 5** Experimental demonstration of a scalable phase modulator. Measured angular differential phase spectra (phase difference between *p*- and *s*-polarization) of Ag/$Sb_2S_3$/ITO stack when $Sb_2S_3$ is in (a) amorphous phase and (b) crystalline phase. (c) Measured reflection spectrum of amorphous and crystalline Ag/$Sb_2S_3$/ITO stack at 62º incident angle for *p*- and *s*-polarization. (d) Measured differential phase spectrum of amorphous and crystalline Ag/$Sb_2S_3$/ITO stack at 62º incident angle. Amp: amorphous and Cry: crystalline